Nonlinear Control of a Planar Magnetic Levitation System

Michel Lévis and Manfredi Maggiore†
Department of Electrical and Computer Engineering
University of Toronto, Toronto ON, Canada, M5S 3G4
{levis,maggiore}@control.utoronto.ca

***Abstract*— This paper initiates a research aimed at developing tools that may have practical significance in contactless position control applications such as, e.g., photolithography. We describe a simple three-magnets planar positioning device, its mathematical model, and design a nonlinear controller that stabilizes it about an equilibrium. Specifically, we derive a feedback transformation mapping the nonlinear system with three positive inputs into a linear system in Brunovsky normal form with two inputs. Robust and robust adaptive controllers are then designed in the transformed input domain and their effectiveness in handling uncertainties is compared through simulations. An experimental testbed under construction is described and will be used as a benchmark to test the controllers developed here as well as other nonlinear control approaches.**

I. INTRODUCTION

Recent trends in the semiconductor industry show an increasing need to refine the photolithography process and achieve smaller linewidths (less than 0.13μm). Currently in industry the photolithography stage is comprised of a lower-stage that actuates large high-speed movements and a flexure-based upper-stage that delivers high-precision movements in multiple degrees of freedom [7]. The mechanical contacts can introduce impurities that may limit the accuracy of the photolithography process, thus decreasing production throughput. Further, the upper-stage flexure mechanism is driven by piezoelectric actuators that are capable of fine resolution but possess severe hysteresis nonlinearity [7]. Mechanical contact problems and the inherent nonlinearities of piezoelectric actuators can be avoided by using planar magnetic levitation technology to move the platen.

Perhaps among the most successful research in this direction is the one reported by Trumper and colleagues in [6], where the authors use a linear controller to actuate a 6 DOF magnetic levitation device that achieves planar motions of up to 50×50 mm^2 using linear motors. Linear motors are indeed particularly suitable for magnetic levitation applications due to their superior range of operation.

Electromagnets can also be used for magnetic levitation, they are cheaper to build, easier to control than linear motors, but typically suffer from a smaller range of operation. This drawback becomes particularly evident when controlling them with linear controllers derived by linearizing the system dynamics about a desired operating condition, since in this case the range of operation and the robustness versus uncertainties are affected. This paper focuses on a planar magnetic levitation device which employs standard electromagnets to achieve 2 DOF, while keeping a relatively large operating range. To avoid the limitations mentioned above, we develop a rigorous nonlinear control framework to solve the stabilization problem over a guaranteed range, and apply robust adaptive control techniques (see [3]) to make the closed-loop system robust versus a class of uncertainties.

We consider the triangular arrangement shown in Figure 1, which has the advantage of minimizing the number of electromagnets needed to actuate two degrees of freedom. Figure 1 illustrates a plan view of the system and the forces exerted on the disk by each magnet. Each of the rectangles represents an electromagnet with a ferromagnetic core with coil windings. The circle in the middle of the plane is a disk, also of ferromagnetic material, whose position we want to control. The vertical airgap of the disk can be controlled independently by a fourth electromagnet suspended over this plane. Since the vertical dynamics are decoupled from the horizontal ones, we focus our attention on the coupled nonlinear subsystem at the base.

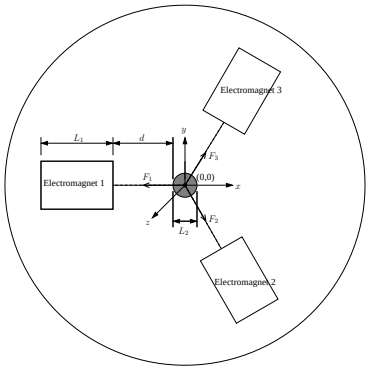

Fig. 1. Forces acting on disk when at origin.

II. MODEL

The equations describing the motion of the disk are

$$\begin{aligned} \ddot{x} &= \frac{F_x(x, y, I_1, I_2, I_3)}{m} \\ \ddot{y} &= \frac{F_y(x, y, I_1, I_2, I_3)}{m}. \end{aligned} \tag{1}$$

The forces F_x and F_y are generated by the electromagnets in the x and y direction, respectively. Notice that the force in the x direction is governed by the disk's y position and

†This work was supported by the Natural Sciences and Engineering Research Council of Canada (NSERC).

the force in the y direction is governed by the disk's x position. In this section we give a mathematical model of the system depicted in Figure 1 using superposition of the forces and neglecting the fringing effect of the magnetic flux lines. The analysis is standard and the result can be found, e.g. in [1] and [8]. Using the state definition

$$\mathbf{x} = \begin{bmatrix} x_1 & x_2 & x_3 & x_4 \end{bmatrix}^\top := \begin{bmatrix} x & \dot{x} & y & \dot{y} \end{bmatrix}^\top, \quad (2)$$

the state-space representation of the system motion dynamics is

$$\begin{aligned}
\dot{x}_1 &= x_2 \\
\dot{x}_2 &= -\frac{1}{2m\mu_o A_1}\Big[\varphi_1(\cdot)(x_1+d)I_1^2 + \varphi_2(\cdot)\left(x_1 - \frac{d}{2}\right)I_2^2 \\
&\quad + \varphi_3(\cdot)\left(x_1 - \frac{d}{2}\right)I_3^2\Big] \\
\dot{x}_3 &= x_4 \\
\dot{x}_4 &= -\frac{1}{2m\mu_o A_1}\Big[\varphi_1(\cdot)(-x_3)I_1^2 + \varphi_2(\cdot)\left(x_3 + \frac{\sqrt{3}}{2}d\right)I_2^2 \\
&\quad + \varphi_3(\cdot)\left(x_3 - \frac{\sqrt{3}}{2}d\right)I_3^2\Big]
\end{aligned} \quad (3)$$

where

$$\begin{aligned}
\varphi_1(x_1,x_3) &= \frac{N_1^2}{\left(\frac{L_1}{\mu_1 A_1} + \frac{L_2}{\mu_2 A_2} + \frac{z_1}{\mu_0 A_1}\right)^2 z_1} \\
\varphi_2(x_1,x_3) &= \frac{N_2^2}{\left(\frac{L_1}{\mu_1 A_1} + \frac{L_2}{\mu_2 A_2} + \frac{z_2}{\mu_0 A_1}\right)^2 z_2} \\
\varphi_3(x_1,x_3) &= \frac{N_3^2}{\left(\frac{L_1}{\mu_1 A_1} + \frac{L_2}{\mu_2 A_2} + \frac{z_3}{\mu_0 A_1}\right)^2 z_3},
\end{aligned}$$

and the vector air gaps are $z_1 = \sqrt{(x_1+d)^2 + x_3^2}$, $z_2 = \sqrt{(x_1 - d/2)^2 + (x_3 + \sqrt{3}/2 \cdot d)^2})$, and $z_3 = \sqrt{(x_1 - d/2)^2 + (x_3 - \sqrt{3}/2 \cdot d)^2}$. Table I lists values of various physical constants in the system used for simulations and other analysis, some are depicted in Figure 1. The length of each core is L_1, their cross-sectional area is A_1 and they have a magnetic permeability of $\mu_1 = \mu_r \mu_0$, where μ_0 is the permeability of free space and μ_r is the relative permeability associated with the material. Electromagnet i, for $i = 1, 2, 3$, has N_i coils windings. The disk has a diameter L_2, a cross-sectional area of A_2 and a magnetic permeability of $\mu_2 = \mu_r \mu_0$. As depicted in Figure 1, the air gap between the face of the cores and the edge of the disk is d when the disk is at the origin. The control inputs are the currents I_1, I_2 and I_3 of the electromagnets.

III. NONLINEAR CONTROL DESIGN

This section demonstrates the design of three nonlinear controllers - an *ideal* controller that stabilizes the uncertainty-free model (1) and robust and robust adaptive controllers that stabilize the system affected by uncertainties. Uncertainties in this system are represented as follows

Parameter	Value
μ_0	$4\pi \times 10^{-7}$
μ_r	700
μ_1	$2.8\pi \times 10^{-4}$
μ_2	$2.8\pi \times 10^{-4}$
L_1	0.1000 m
L_2	0.0167 m
d	0.0500 m
m	0.5000 kg
h	0.0083 m
N	100
A_1	0.01 m^2
A_2	1.39×10^{-4} m^2

TABLE I
VALUES OF PHYSICAL PARAMETERS.

$$\begin{aligned}
\dot{x}_1 &= x_2 \\
\dot{x}_2 &= \frac{F_x(x_1,x_3,I_1,I_2,I_3)}{m} + \delta_2(x_1,x_2,x_3) \\
\dot{x}_3 &= x_4 \\
\dot{x}_3 &= \frac{F_y(x_1,x_3,I_1,I_2,I_3)}{m} + \delta_4(x_1,x_3,x_4),
\end{aligned} \quad (4)$$

where $\delta_2(x_1,x_2,x_3)$ and $\delta_4(x_1,x_3,x_4)$ represent unknown forces (i.e. accelerations) that can be generated from various electromagnetic modelling assumptions not holding, as well as friction. Such unknown forces are assumed to have structurally known upper bound as follows

$$\begin{aligned}
\delta_2(\cdot) &= \Delta_2(x_1,x_3) - \theta_3 x_2, \ |\Delta_2(\cdot,\cdot)| \le \theta_1 |x_1| + \theta_2 |x_3| \\
\delta_4(\cdot) &= \Delta_4(x_1,x_3) - \theta_6 x_4, \ |\Delta_4(\cdot,\cdot)| \le \theta_4 |x_1| + \theta_5 |x_3|
\end{aligned} \quad (5)$$

where $\theta_i \in \mathbb{R}^p$, for $i = \{1, .., 6\}$, are unknown parameters and the terms $-\theta_3 x_2$, $-\theta_6 x_4$ represent viscous friction.

A. Ideal Control Design

In this section, the design of a nonlinear controller that provides asymptotic stabilization to the origin is described. The ideal controller does not take uncertainties into account, thus here it is assumed that $\delta_2 = 0$ and $\delta_4 = 0$.

Proposition 1: *There exists a feedback transformation for (3),*

$$[I_1^2 \ I_2^2 \ I_3^2]^\top = T(\mathbf{x}, \mathbf{u}),$$

where $\mathbf{u} = [u_1, u_2]^\top$ *and* $T : \mathbb{R}^4 \times \mathbb{R}^2 \to \mathbb{R}^3$ *is well-defined over the set*

$$\mathbf{C} = \left\{ \mathbf{x} \in \mathbb{R}^4, \mathbf{u} \in \mathbb{R}^2 : |x_1| \le \frac{d}{6}, \ |x_3| \le \frac{d}{6} \right\}, \quad (6)$$

such that the dynamics in the transformed input domain read as

$$\begin{aligned}
\dot{x}_1 &= x_2 \quad \dot{x}_3 = x_4 \\
\dot{x}_2 &= u_1 \quad \dot{x}_4 = u_2,
\end{aligned} \quad (7)$$

where u_1 and u_2 are the new control inputs after feedback transformation.

Remark 1: Note that the feedback transformation in Proposition 1 is not a standard feedback linearizing one in that while the original system (3) has three positive inputs, the transformed system (7) is linear with two inputs.

The solution presented here is a generalization of an idea presented in [5], Section 12.3. Due to space limitations, the proof will be omitted. We use the following transformation to fulfill Proposition 1

$$\begin{aligned} I_1^2 &= \frac{-2m\mu_0 A_1}{\varphi_1(\cdot)(x_1+x_3+d)}\,\eta_1(x_1,x_3,u_1,u_2) \\ I_2^2 &= \frac{-2m\mu_0 A_1}{\varphi_2(\cdot)\Big(x_1-x_3-\frac{\sqrt{3}+1}{2}d\Big)}\,\eta_2(x_1,x_3,u_1,u_2) \\ I_3^2 &= \frac{-2m\mu_0 A_1}{\varphi_3(\cdot)\Big(x_1-x_3+\frac{\sqrt{3}-1}{2}d\Big)}\,\eta_3(x_1,x_3,u_1,u_2), \end{aligned} \tag{8}$$

where for an $\epsilon > 0$, $\eta_1(x_1,x_3,u_1,u_2)$, $\eta_2(x_1,x_3,u_1,u_2)$ and $\eta_3(x_1,x_3,u_1,u_2)$ are

$$\begin{aligned} \eta_1(\cdot) &= \frac{u_1-u_2-\sqrt{(u_1-u_2)^2+\epsilon}}{4} - A(\cdot) \\ \eta_2(\cdot) &= \frac{u_1-u_2+\sqrt{(u_1-u_2)^2+\epsilon}}{2} + A(\cdot) + B(\cdot) \\ \eta_3(\cdot) &= \frac{u_1-u_2-\sqrt{(u_1-u_2)^2+\epsilon}}{4} - B(\cdot). \end{aligned}$$

The positive functions $A(x_1,x_3,u_1,u_2)$ and $B(x_1,x_3,u_1,u_2)$ are defined as

$$\begin{aligned} A(x_1,x_3,u_1,u_2) &= -\frac{1}{f_a(\cdot)}\left(f_{\text{pos}}(\cdot) + \frac{-u_1+\sqrt{u_1^2+\epsilon}}{2}\right) \\ B(x_1,x_3,u_1,u_2) &= -\frac{1}{f_b(\cdot)}\left(f_{\text{neg}}(\cdot) + \frac{-u_1-\sqrt{u_1^2+\epsilon}}{2}\right) \end{aligned}$$

where $f_a(x_1,x_3)$, $f_b(x_1,x_3)$, $f_{\text{neg}}(x_1,x_3)$, and $f_{\text{pos}}(x_1,x_3)$ are

$$\begin{aligned} f_a(\cdot) &= \frac{x_1-\frac{d}{2}}{x_1-x_3-\frac{\sqrt{3}+1}{2}d} - \frac{x_1+d}{x_1+x_3+d} \\ f_b(\cdot) &= \frac{x_1-\frac{d}{2}}{x_1-x_3-\frac{\sqrt{3}+1}{2}d} - \frac{x_1-\frac{d}{2}}{x_1-x_3+\frac{\sqrt{3}-1}{2}d} \\ f_{\text{neg}}(\cdot) &= \frac{u_1-u_2-\sqrt{(u_1-u_2)^2+\epsilon}}{4}\left(\frac{x_1+d}{x_1+x_3+d}\right) \\ f_{\text{pos}}(\cdot) &= \frac{u_1-u_2-\sqrt{(u_1-u_2)^2+\epsilon}}{4}\,\frac{x_1-\frac{d}{2}}{x_1-x_3+\frac{\sqrt{3}-1}{2}d} \\ &\quad + \frac{u_1-u_2+\sqrt{(u_1-u_2)^2+\epsilon}}{2}\,\frac{x_1-\frac{d}{2}}{x_1-x_3-\frac{\sqrt{3}+1}{2}d}. \end{aligned}$$

Note that for all $(\mathbf{x},\mathbf{u}) \in \mathbf{C}$ (defined in (6)), $f_{\text{neg}} < 0$, $f_{\text{pos}} > 0$, $f_a < 0$ and $f_b > 0$. After the feedback transformation in (8), system (3) reads as (7) which is in Brunovsky normal form. To stabilize the origin we can, e.g., employ a LQR controller, $\mathbf{u} := [u_1,u_2]^\top = -\mathbf{K}\mathbf{x}$, in the transformed input domain. For our simulations we choose

$$\mathbf{Q} = diag\{5000,100,700,2000\}, \mathbf{R} = \begin{bmatrix} 5000 & 1000 \\ 1000 & 5000 \end{bmatrix}. \tag{9}$$

The design of a nonlinear stabilizer in the absence of uncertainties is now complete.

B. Robust Control Design

In this section we robustify the controller developed in the previous section to account for the uncertainties in (4). To this end, using the feedback transformation (8), (4) is mapped to

$$\dot{\mathbf{x}} = \begin{bmatrix} 0 & 1 & 0 & 0 \\ 0 & 0 & 0 & 0 \\ 0 & 0 & 0 & 1 \\ 0 & 0 & 0 & 0 \end{bmatrix}\mathbf{x} + \begin{bmatrix} 0 & 0 \\ 1 & 0 \\ 0 & 0 \\ 0 & 1 \end{bmatrix}(\mathbf{u}+\delta(\mathbf{x})) \tag{10}$$

where $\delta(\mathbf{x}) = [\delta_2(x_1,x_2,x_3),\delta_4(x_1,x_3,x_4)]^\top$. Since the uncertainty δ satisfies a matching condition, Lyapunov redesign is a natural choice for robust stabilization. Following the standard Lyapunov redesign technique (see, e.g., [2]), we replace the linear controller (in the transformed input domain) developed in the previous section, $\mathbf{u} = -\mathbf{K}\mathbf{x}$, by $\mathbf{u} = -\mathbf{K}\mathbf{x} + \mathbf{v}$, where $\mathbf{v}$ is to be designed to achieve practical stability of the origin $\mathbf{x} = 0$ (i.e., stability of a residual set around the origin which can be made arbitrarily small). In order to do that, we use the inequalities in (5) and assume that we know two positive scalars β_1 and β_2 satisfying

$$|\theta_i| \le \beta_1,\ i = 1,2,4,5, \qquad |\theta_j| \le \beta_2,\ j = 3,6.$$

An upper bound to $\|\delta(\mathbf{x})\|_2$ is thus given by

$$\begin{aligned} \|\delta(\mathbf{x})\|_2 &= \left(|\delta_2|^2 + |\delta_4|^2\right)^{\frac{1}{2}} \\ &\le \left(2\beta^{*^2}(|x_1|+|x_3|)^2 + 2\beta^{*^2}(|x_1|+|x_3|)(|x_2|+|x_4|)\right. \\ &\quad \left. + \beta^{*^2}\left(x_2^2+x_4^2\right)\right)^{\frac{1}{2}} \\ &:= \rho(\mathbf{x}) \end{aligned}$$

where $\beta^* = \max\{\beta_1,\beta_2\}$. Next, defining $\mathbf{v}$ as

$$\mathbf{v} = \begin{cases} -\eta(\mathbf{x})\frac{\omega}{\|\omega\|_2} & \text{if } \eta(\mathbf{x})\|\omega\|_2 \ge \gamma \\ -\eta(\mathbf{x})^2\frac{\omega}{\gamma} & \text{if } \eta(\mathbf{x})\|\omega\|_2 < \gamma \end{cases} \tag{11}$$

where $\gamma > 0$, the resulting closed-loop trajectories converge to a neighborhood of order γ about the origin. This completes the robust nonlinear control design. Simulation results of the robust controller are shown in Section IV.

C. Robust Adaptive Control Design

Although the robust control controller developed in the previous section guarantees stability for the system subject to uncertainties δ_2 and δ_4 in (4), it does have practical drawbacks. Specifically, the currents have a high-frequency component due to the fact that (11) is a smoothed version of

a sliding mode controller. Further, a robust controller may require a large control effort which is not desirable in the application under consideration because of the saturation limits of the amplifiers. Both the drawbacks above may, in principle, be overcome by designing an adaptive controller. However, adaptive control designs would typically require the uncertainties in (4) to be structured, i.e., to exactly match the structure the adaptive control design calls for, and most often to be linear with respect to unknown parameters. Uncertainties δ_2 and δ_4 in (5) cannot be assumed to be structured and to be linear functions of unknown parameters (although, such an assumptions are reasonable for the friction terms).

In the light of the above we choose to develop a robust adaptive control that handles friction in the classic adaptive manner but compensates uncertainties Δ_2 and Δ_4 using adaptive upper bounds. To this end, we employ the technique developed by Polycarpou and Iannou in [3], which ensures that the trajectories of the closed-loop system are globally uniformly ultimately bounded (GUUB) with a small ultimate bound. The methodology in [3] applies to the class of nonlinear systems

$$\begin{aligned}\dot{x}_i &= x_{i+1} + \theta^\top \varphi_i(x_1, ..., x_i) + \Delta_i(\mathbf{x}, t),\ 1 \le i \le n-1\\ \dot{x}_n &= u + \theta^\top \varphi_n(\mathbf{x}) + \Delta_n(\mathbf{x}, t),\end{aligned} \tag{12}$$

where $\theta_1, \ldots, \theta_n$ are unknown scalar parameters, $\varphi_1, \ldots, \varphi_n$ are known smooth functions and $\Delta_1, \ldots, \Delta_n$ are unknown functions that satisfy A1.

Assumption A1(Triangularity Condition): There exists, possibly unknown, parameters $\psi_i \in \mathbb{R} \ge 0$ and known smooth functions $p_i : \mathbb{R}^i \to \mathbb{R}^+ \backslash \{0\}$ such that for all $x \in \mathbb{R}^n$ and $t \in \mathbb{R}^+$

$$|\Delta_i(\mathbf{x}, t)| \le \psi_i p_i(x_1, ..., x_i),\ 1 \le i \le n. \tag{13}$$

After applying the nonlinear input transformation (8) to the uncertain system (4), we get (10) where $\delta_2(x_1, x_2, x_3)$ and $\delta_4(x_1, x_3, x_4)$ are defined in (5). Letting

$$\begin{aligned}u_1 &:= x_3\\ \varphi_1 &:= \begin{bmatrix} 0 & 0 & 0 & 0 \end{bmatrix}^\top\\ \varphi_2 &:= \begin{bmatrix} 0 & -x_2 & 0 & 0 \end{bmatrix}^\top\\ \varphi_3 &:= \begin{bmatrix} 0 & 0 & 0 & 0 \end{bmatrix}^\top\\ \varphi_4 &:= \begin{bmatrix} 0 & 0 & 0 & -x_4 \end{bmatrix}^\top,\end{aligned}$$

we have that (10) fits the structure in (12). Next, in order for A1 to be satisfied we need to impose the requirement that $\theta_2 = 0$, and we need to find a smooth upper bound to $|\Delta_2(x_1, x_3)|$ (the function $\theta_2|x_3|$ is not smooth). Noticing that for any $c_1 > 0$, there exist scalars $\psi_2 > 0$ such that

$$\theta_1|x_1| \le \psi_2(x_1^2 + c_1),$$

and setting

$$p_2(x_1) = x_1^2 + 1.65,$$

we have that A1 is satisfied. The imposed requirement that $\theta_2 = 0$ poses a limitation to the generality of the solution presented here and its impact on the performance of the experimental testbed under construction will be the subject of future investigation. Define the error variables

$$\begin{aligned}z_1 &= x_1\\ z_2 &= x_2 - \alpha_1\\ z_3 &= x_3 - \alpha_2\\ z_4 &= x_4 - \alpha_3.\end{aligned}$$

using the stabilization functions

$$\begin{aligned}\alpha_1 &= -k_1 z_1\\ \alpha_2 &= -z_1 - k_2 z_2 + \frac{\partial \alpha_1}{\partial x_1} x_2 - \hat{\theta}^\top \varphi_2 - \hat{\psi}_2 \omega_2\\ \alpha_3 &= -z_2 - k_3 z_3 + \frac{\partial \alpha_2}{\partial x_1} x_2 + \frac{\partial \alpha_2}{\partial x_2} x_3 + \frac{\partial \alpha_2}{\partial x_2} \hat{\theta}^\top \varphi_2\\ &\quad - \hat{\psi}_3 \omega_3 + \frac{\partial \alpha_2}{\partial \hat{\theta}} \tau_3 + \frac{\partial \alpha_2}{\partial \hat{\psi}_1} \dot{\hat{\psi}}_1 + \frac{\partial \alpha_2}{\partial \hat{\psi}_2} \dot{\hat{\psi}}_2,\end{aligned}$$

where $\hat{\Psi}_i$ is the upper bound estimate, $\hat{\theta}$ is estimate of the friction parameters, and the gains are $k_1 = 1.75$, $k_2 = 1.5$ and $k_3 = 1.75$. The triangular bounds for $\Lambda_3 = -\frac{\partial \alpha_2}{\partial x_2} \Delta_2$ and $\Lambda_4 = \Delta_4 - \frac{\partial \alpha_3}{\partial x_2} \Delta_2$ such that

$$|\Lambda_3| \le \bar{\psi}_3 \bar{p}_3 \le \psi_3^{\mathrm{M}} \bar{p}_3, \qquad |\Lambda_4| \le \bar{\psi}_4 \bar{p}_4 \le \psi_4^{\mathrm{M}} \bar{p}_4,$$

where $\psi_3^{\mathrm{M}} = \max\left\{\bar{\psi}_3, \psi_3^o\right\}$ and $\psi_4^{\mathrm{M}} = \max\left\{\bar{\psi}_4, \psi_4^o\right\}$, are found by choosing the functions

$$\begin{aligned}\bar{p}_3(x_1, x_2, x_3) &= \left[\frac{\partial \alpha_2}{\partial x_2} \tanh\left(10 \frac{\partial \alpha_2}{\partial x_2}\right) + 0.1\right] p_2\\ \bar{p}_4(\mathbf{x}) &= |\Delta_4| + \left|\frac{\partial \alpha_3}{\partial x_2}\right| |\Delta_2| = (|x_1| + |x_3|) \left(1 + \left|\frac{\partial \alpha_3}{\partial x_2}\right|\right)\end{aligned}$$

For $\epsilon_1 = 0.01$, $\epsilon_2 = 10^{-9}$, $\epsilon_3 = 0.01$ and $\epsilon_4 = 10^{-9}$ the smoothed versions of the upper bound functions are $\omega_2 = p_2 \tanh\left[(z_2 p_2)/\epsilon_2\right]$, $\omega_3 = \bar{p}_3 \tanh\left[(z_3 \bar{p}_3)/\epsilon_3\right]$ and $\omega_4 = \bar{p}_4 \tanh\left[(z_4 \bar{p}_4)/\epsilon_4\right]$. Next, the adaptive laws that update the parameters $\hat{\Psi}_i$ and $\hat{\theta}$ are

$$\begin{aligned}\dot{\hat{\psi}}_1(t) &= -\sigma_1 \gamma_1 (\hat{\psi}_1 - \psi_1^0)\\ \dot{\hat{\psi}}_2(t) &= \gamma_2 \left(z_2 \omega_2 - \sigma_2 (\hat{\psi}_2 - \psi_2^0)\right)\\ \dot{\hat{\psi}}_3(t) &= \gamma_3 \left(z_3 \omega_3 - \sigma_3 (\hat{\psi}_3 - \psi_3^0)\right)\\ \dot{\hat{\psi}}_4(t) &= \gamma_4 \left(z_4 \omega_4 - \sigma_4 (\hat{\psi}_4 - \psi_4^0)\right)\\ \tau_3 &= \Gamma \left(-\sigma_\theta (\hat{\theta} - \theta^0) + z_2 \varphi_2 - z_3 \frac{\partial \alpha_2}{\partial x_2} \varphi_2\right)\\ \dot{\hat{\theta}} &= \tau_3 + \Gamma z_4 \left(\varphi_4 - \frac{\partial \alpha_3}{\partial x_2} \varphi_2\right)\end{aligned}$$

where $\gamma_1 = \gamma_2 = \gamma_3 = \gamma_4 = 3.5$, $\sigma_1 = \sigma_2 = \sigma_3 = \sigma_4 = 1$, $\psi_1^o = \psi_2^o = \psi_3^o = \psi_4^o = 0$, $\sigma_\theta = 1$, $\theta^o = \begin{bmatrix} 0 & 0 & 0 & 0 \end{bmatrix}^\top$ and $\Gamma = diag\{3, 3, 3, 3\}$. The final control law that uses the parameter estimates to compensate

for uncertainties is

$$u_2 = -z_3 - k_4 z_4 + \frac{\partial \alpha_3}{\partial x_1} x_2 + \frac{\partial \alpha_3}{\partial x_2} x_3 + \frac{\partial \alpha_3}{\partial x_3} x_4 - \hat{\theta}^\top \left(\varphi_4 - \frac{\partial \alpha_3}{\partial x_2} \varphi_2 \right) - \hat{\psi}_4 \omega_4 + \frac{\partial \alpha_3}{\partial \hat{\theta}} \dot{\hat{\theta}} + \frac{\partial \alpha_3}{\partial \hat{\psi}_1} \dot{\hat{\psi}}_1 + \frac{\partial \alpha_3}{\partial \hat{\psi}_2} \dot{\hat{\psi}}_2 + \frac{\partial \alpha_3}{\partial \hat{\psi}_3} \dot{\hat{\psi}}_3 + \Gamma z_3 \frac{\partial \alpha_2}{\partial \hat{\theta}} \left(\varphi_4 - \frac{\partial \alpha_3}{\partial x_2} \varphi_2 \right),$$

where $k_4 = 1.5$. The robust adaptive controller is simulated in Section IV using the following initial conditions for the update parameter laws

$$\hat{\theta}(0) = \begin{bmatrix} 0 & 0 & 0 & 0 \end{bmatrix}^\top, \hat{\psi}(0) = \begin{bmatrix} 0 & 0 & 0 & 0 \end{bmatrix}^\top,$$

and the various control parameters given throughout this section.

IV. SIMULATION RESULTS

In this section we test in simulation the designs of Sections III-A, III-B, III-C, namely the ideal, robust, and robust adaptive controllers. To compare our nonlinear designs to the approach, often used in the control of electromagnetic devices, of linearizing the system about the desired equilibrium and designing a linear controller, we include in our comparisons a linear controller $[I_1^2, I_2^2, I_3^2]^\top = K_L \mathbf{x}$, where the vector K_L is obtained by applying LQR design to the linearization of the system at the origin, with $\mathbf{Q} = diag\{5000, 100, 700, 2000\}$, $\mathbf{R} = diag\{1000, 100, 1000\}$. Figure 2 depicts the position trajectories when the system is

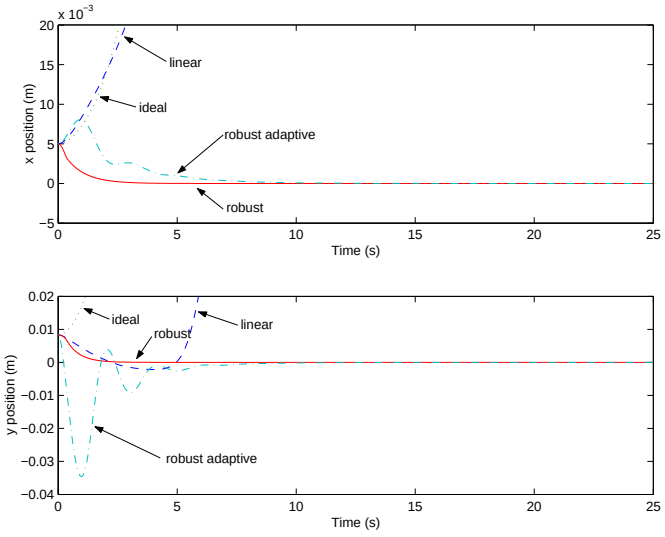

Fig. 2. Response of uncertain system when using a linear controller and the robust nonlinear controller.

subject to uncertainties: $\delta_2(x_1, x_2, x_3) \leq 1.1\,|x_1| - 0.01 x_2$ and $\delta_4(x_1, x_3, x_4) \leq 1.1\,|x_1| + 1.1\,|x_3| - 0.01 x_4$. The linear and ideal controllers do not stabilize the system. The robust controller manages to stabilize the system and achieves a steady-state error of 2.20206×10^{-6} m at a maximum current of 4.0165 A. The robust adaptive controller stabilizes the system with a smaller steady-state error of 1.4299×10^{-7} m but with a higher peak current of 6.2250 A. Although the y trajectory conflicts with the domain $\mathbf{C}$ constraint, defined in (6), the control remains defined, indicating that $\mathbf{C}$ is quite conservative. The current

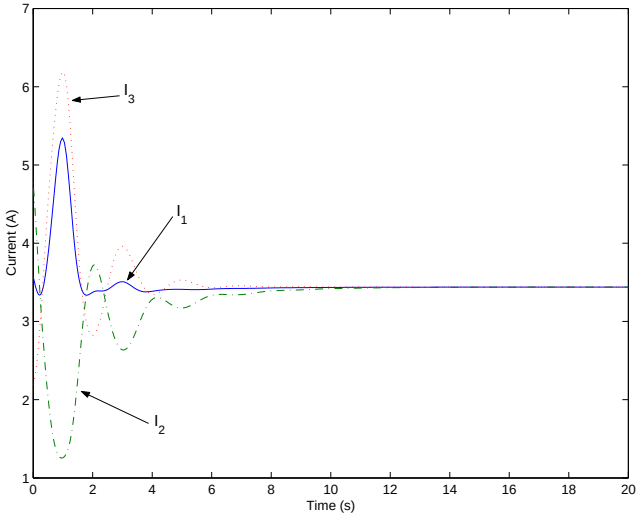

Fig. 3. Currents of robust adaptive nonlinear controller in uncertain system.

plot when using the robust adaptive control is shown above in Figure 3. Using smooth currents, the robust adaptive controller obtains the best steady-state error. However, its peak current is 2.2 A higher than that of the robust controller. On the other hand, the practical issue with using the robust controller is the chattering effect of the control inputs that cannot be realized in hardware and can also excite high-frequency unmodelled dynamics in the system [4].

V. IMPLEMENTATION

The prototype of the planar magnetic levitation device has been built, shown in Figure 4 and Figure 5. Unfortunately due to hardware limitations, the device cannot yet be used to test the nonlinear controllers developed in this paper and serve as a benchmark to test other nonlinear control approaches.

The electromagnet cores, shown in Figure 4, have a cross sectional area of 5×5 cm^2 and are 40 cm long. These dimensions were chosen to obtain substantial strength from inefficient rectangular magnets (see e.g., [1]). Each magnet's strength is further increased by using laminated cores made of low-copper soft steel. They are wound with 22-Gauge magnet wire and the inductance of each electromagnet is about 40 mH. Coil dynamics can be ignored by using a simple PI current controller and driving each electromagnet with a commercial PWM amplifier.

Including an additional magnet in the z direction for vertical levitation would increase expenses without making the control problem more interesting since the force in the z direction is decoupled from those acting in the xy plane. For this reason we suspended the disk by a wooden

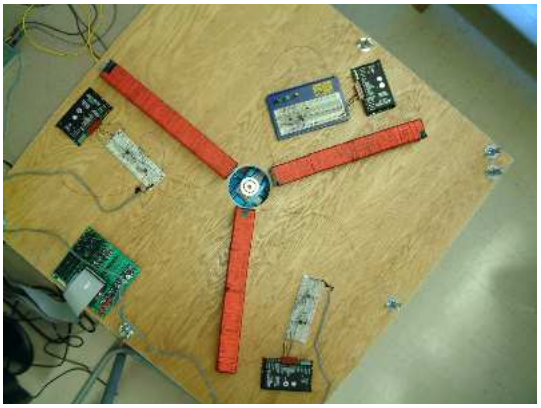

Fig. 4. Top view of planar magnetic levitation prototype.

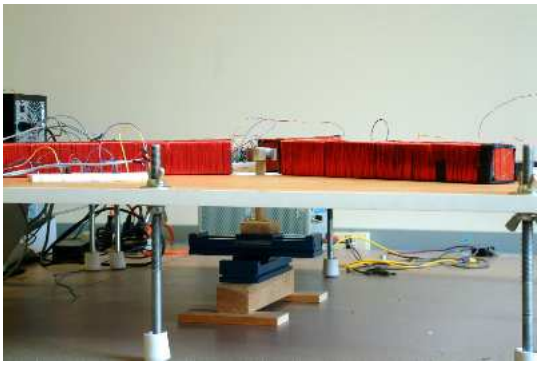

Fig. 5. Side view of planar magnetic levitation prototype.

dowel anchored onto the small platform of a linear guide, as shown in Figure 5. Linear guides are constructed of a lightweight alloy and consist of a platform that rides on ball bearings for low-friction movement. Two such linear guides are placed one on top of the other perpendicularly so that low-friction planar movement is obtained.

Measuring the x and y positions of the disk cannot be done using most optical, transducer, and capacitive sensors. Optical solutions such as laser interferometers are usually used on targets with a flat body and would give false readings off the disk's curved surface. Transducer and capacitive sensors rely on magnetic or electric fields to get their measurement and thus the electromagnetic field generated by the electromagnets may interfere with those of the sensors and cause false readings. High-resolution measurements of the disk's (x, y) position can be obtained by mounting optical encoders on the platform of each linear guide and attaching their shafts with a fishing line that is fastened at each end of the guides. This solution is inexpensive and provides resolution of the order of 5 μm.

The nonlinear controllers will be tested using the Wincon software platform by Quanser Consulting. The encoder inputs, actual current readings and controller reference current outputs are interfaced through the Quanser MultiQ PCI data acquisition card.

VI. CONCLUSIONS

We developed nonlinear controllers stabilizing the model of a planar magnetic levitation device and briefly discussed its implementation. The nonlinear controller developed has difficulty overcoming the Coulomb friction introduced by the linear guides without saturating the actuators. Therefore, larger power amplifiers are required and hardware design changes are needed to reduce or even completely remove friction. It is also recommended that a more magnetically permeable core material is used. After modifying the experimental testbed to avoid the problems indicated above, the device will be used to investigate the limitations of the various controllers presented here, as well as to test other ideas. Future research will focus on the design and implementation of improved robust stabilizing controllers and robust tracking controllers for this testbed.

ACKNOWLEDGEMENTS

The authors would like to thank J.T. Spooner for providing inspiration for some of the ideas contained in this paper. Jacob Apkarian and Peter Lehn for their many helpful remarks on the implementation of the experimental testbed. V.M. Alexander and Al Shabia Engineering, Sharjah, U.A.E., for supplying and designing the electromagnet cores. Marcel Lévis for building the platform and various other items needed in the implementation.

VII. REFERENCES

[1] Kenneth D. Demarest, *Engineering electromagnetics*, Prentice Hall, New Jersey, 1998.

[2] Hassan K. Khalil, *Nonlinear systems*, second ed., Prentice Hall, Upper Saddle River, NJ 07458, 1995.

[3] M. M. Polycarpou and P. A. Ioannou, *A robust adaptive nonlinear control design*, Automatica **32** (1996), 423–427.

[4] Jean-Jackques E. Slotline and Weiping Li, *Applied nonlinear control*, first ed., Prentice Hall, Englewood Cliffs, NJ 07632, 1991.

[5] J.T. Spooner, M. Maggiore, R. Ordóñez, and K.M. Passino, *Stable adaptive control and estimation for nonlinear systems: Neural and fuzzy approximator techniques*, John Wiley & Sons, New York, 2002.

[6] David L. Trumper, *Modeling and vector control of planar magnetic levitator*, IEEE Transactions on Industry Applications **34** (1998), 1254–1262.

[7] Kuen-Yu Tsai and Jia-Yush Yen, *Servo system design of a high-resolution piezo-driven fine stage for step-and-repeat microlithography systems*, The 25th Annual Conference of the IEEE Industrial Electonics Society **1** (1999), 11–16.

[8] Herbert H. Woodson and James R. Melcher, *Electromechanical dynamics*, John Wiley & Sons, Inc., New York, 1968.